NANO LETTERS

Letter

Ballistic Phonons in Ultrathin Nanowires

Daniel Vakulov,[⊥] Subash Gireesan,[⊥] Milo Y. Swinkels,[⊥] Ruben Chavez, Tom Vogelaar, Pol Torres, Alessio Campo, Marta De Luca, Marcel A. Verheijen, Sebastian Koelling, Luca Gagliano, Jos E. M. Haverkort, F. Xavier Alvarez, Peter A. Bobbert, Ilaria Zardo, and Erik P. A. M. Bakkers*

Read Online

ACCESS | Metrics & More | Article Recommendations | Supporting Information

ABSTRACT: According to Fourier's law, a temperature difference across a material results in a linear temperature profile and a thermal conductance that decreases inversely proportional to the system length. These are the hallmarks of diffusive heat flow. Here, we report heat flow in ultrathin (25 nm) GaP nanowires in the absence of a temperature gradient within the wire and find that the heat conductance is independent of wire length. These observations deviate from Fourier's law and are direct proof of ballistic heat flow, persisting for wire lengths up to at least 15 μm at room temperature. When doubling the wire diameter, a remarkably sudden transition to diffusive heat flow is observed. The ballistic heat flow in the ultrathin wires can be modeled within Landauer's formalism by ballistic phonons with an extraordinarily long mean free path.

KEYWORDS: Nanowires, GaP, heat transport, ballistic phonons, Raman spectroscopy
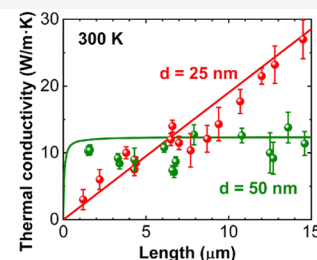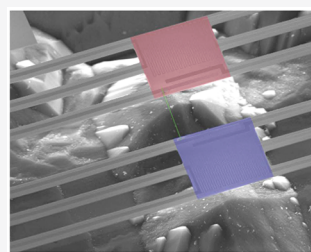
Heat flow in macroscopic systems is traditionally described by Fourier's law for diffusive heat flow.[1] The advancement of micro and nanotechnology has led in the past few years to observations of nondiffusive heat flow. Deviations from diffusive heat flow can occur due to the wave nature of phonons,[2] hydrodynamic effects,[3−10] and ballistic behavior.[11−18] In nanowires (NWs), scattering of phonons at the NW surface reduces the thermal conductivity as compared to the bulk.[19] However, when the surface is atomically flat, phonons may reflect specularly from the surface[20,21] and ballistic heat flow in the axial direction may occur.

Realizing ballistic flow over large distances at room temperature requires a long phonon mean free path (MFP), which is challenging due to different scattering mechanisms. Only a few studies have reported the observation of ballistic transport at room temperature. Ballistic transport at room temperature up to a length of 260 nm was reported in short and wide graphene ribbons.[12] The heat transport is diffusive in short and narrow ribbons due to the presence of edge disorder. Room-temperature ballistic heat flow up to a length of 8.3 μm was reported for SiGe NWs with diameters in the range 50−200 nm.[13] Its occurrence was attributed to the filtering out of high-frequency short-MFP phonons by alloy scattering. Beyond 8.3 μm, the heat flow in these NWs was found to be diffusive. Ballistic phonon transport at room temperature was also reported in holey silicon up to a length of 200 nm.[15] The explanation in this case was that surface disorder filters out high-frequency phonons, leaving the ballistic transport of low-frequency phonons.

In this letter, we demonstrate room-temperature axial ballistic heat flow in ultrathin, 25 nm diameter, GaP NWs up to wire lengths of at least 15 μm, and a sharp transition to diffusive heat flow when the diameter is doubled to 50 nm. Room-temperature ballistic transport over such large distances and a diffusive-ballistic transition with decreasing lateral dimension have not been reported thus far. The temperature profile along the NWs is obtained by Raman thermometry, confirming the presence of a temperature gradient in the diffusive flow regime and its absence in the ballistic regime.

We grow GaP NWs with 25−140 nm diameters by metal−organic vapor-phase epitaxy using the vapor−liquid−solid growth technique (see Supplementary Section SI1). The NWs are grown in arrays by substrate/catalyst patterning. Within an array, the NWs have a uniform diameter along their length with a <5 nm diameter spread. We analyze the structural properties of the NWs by transmission electron microscopy (TEM). TEM images show stacking-fault-free NWs, grown along the ⟨0001⟩ direction (see Figure 1a). The NWs have atomically flat {1100} side facets covered by an approximately 2 nm-thick amorphous oxide layer (see Figure 1b). Electron diffraction patterns taken in the TEM further show that NWs
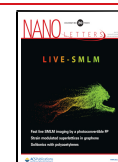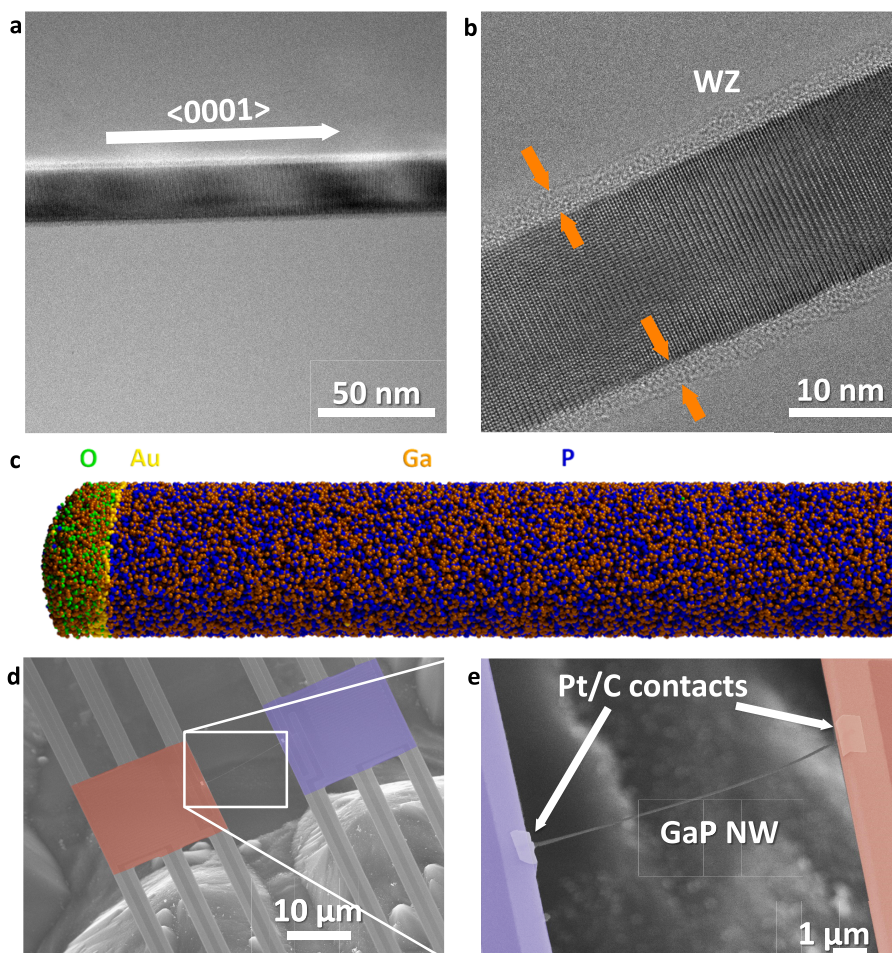
Figure 1. GaP NW properties and device for thermal conductance measurements. (a) TEM image of a 25 nm diameter GaP NW, grown along the $\langle 0001 \rangle$ direction. (b) High-resolution TEM image taken along the $\langle 11\bar{2}0 \rangle$ direction of a NW, showing a defect-free WZ crystal structure and a layer of oxide (orange arrows). (c) APT analysis of a 25 nm diameter NW showing its high chemical purity. (d) 45°-tilted SEM image of the thermal conductance measuring device, with suspended heating (red) and sensing (blue) membranes. (e) Zoom-in of the GaP NW bridging the suspended membranes. Electron beam-induced deposited Pt/C improves the thermal contact.

with different diameters used in our study all have a wurtzite (WZ) crystal structure (see Figure S1). Atom-probe tomography (APT) demonstrates the chemical purity of the NWs and the absence of heavy element impurities (see Figures 1c and S2). The NWs are therefore atomically clean and defect-free. Our GaP NWs are thus ideal systems to look for ballistic heat transport. Limitations of the APT technique prevent detection of the oxide layer.[22] We fabricate microdevices[23,24] to study the thermal conductivity of individual NWs (see Section SI3). The devices consist of two suspended membranes with Pt meander structures on top, which can be used as heater and thermometer; see the scanning electron microscopy (SEM) picture in Figure 1d. Different spacings between the membranes allow measuring NWs of different lengths. Using a micromanipulator under an optical microscope, we place as-grown single NWs with selected diameter between the membranes. Pt/C contacts are deposited on top of the NWs to improve the thermal contact (see Figure 1e). We determine the thermal conductivity κ from the measured thermal conductance G and the NW dimensions. The thermal conductance of the NW, which is defined as the amount of heat flux going through a material when one Kelvin temperature difference is applied, is determined by applying

a current to one of the coils and measuring the temperature on both sides of the NW. From these measurements, the NW thermal conductance is extracted through a heat balance calculation for the sensing membrane, where the heat transported through the wire is put equal to the heat that leaves the membrane through the SiN_x beams, as is commonly done when employing this kind of devices (see Section SI3 and ref 23.).

The extracted κ at room temperature $T = 300$ K is plotted in Figure 2a as a function of diameter d for NWs with approximately the same length $L = 6.7 \pm 0.1$ μm, with d ranging from 25 to 140 nm. These results were fitted to expose the influence of the thermal contact resistance, R_c.[24] In a NW with heat flow dominated by diffuse scattering at the NW surface, κ increases with d according to Mathiessen's rule $\kappa \propto (1 + l_{bulk}/d)^{-1}$, where l_{bulk} is the bulk MFP, as indicated by the dashed line. A reduced κ with respect to this line, which is observed for $d \geq 75$ nm, indicates that R_c is no longer negligible compared to the NW resistance.[24] For thin wires ($d < 50$ nm), on the contrary, an enhanced κ is observed, indicating that a nondiffusive transport mechanism, not dominated by a contact resistance, becomes progressively important with decreasing diameter. To investigate the
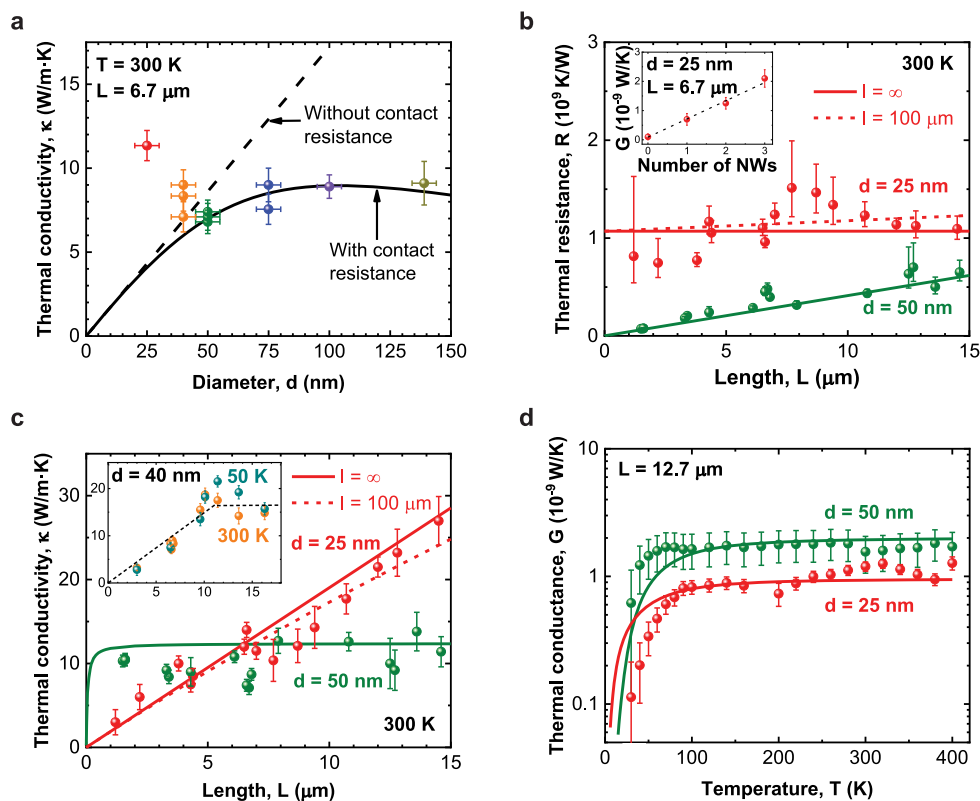
Figure 2. Transition from diffusive to ballistic heat flow. (a) Room-temperature (300 K) thermal conductivity κ of GaP NWs of length $L = 6.7 \pm 0.1$ μm as a function of diameter d. Full curve: Fit of results for $d \geq 50$ nm to $\kappa = (1/c_1 d + c_2 \pi d/4L)^{-1}$ (diffusive heat flow with MFP $l = d \ll l_{bulk}$ and contact resistance $R_c = c_2/d$, with $c_1 = 1.7 \times 10^8$ W/m^2·K and $c_2 = 4.6$ m·K/W). Dashed line: $\kappa = c_1 d$ (diffusive heat flow without contact resistance and $d \ll l_{bulk}$). (b) Symbols: Measured length dependence of resistance R of NWs with $d = 25$ and 50 nm. Lines: Modeling results based on Landauer's formalism, using the numbers of specular phonon modes N_s ($d = 25$ nm, solid line: MFP $l = \infty$, dashed line: $l = 100$ μm) and diffusive phonon modes N_d ($d = 50$ nm, MFP $l = d$) from Figure S12. For $d = 25$ nm, the curve for $l = 100$ μm is obtained by dividing the result for $l = \infty$ by the transmission coefficient $l/(l + L)$.[30] Inset: Conductance G of a device without a NW (see Section SI4) and with 1, 2, and 3 NWs with $d = 25$ nm and $L = 6.7 \pm 0.1$ μm. Dashed line: Linear fit. (c) Same results as in main panel of (b), but for the conductivity κ. Inset: Results for $d = 40$ nm NWs measured at 300 and 50 K (measurements on different devices at the different temperatures). Dashed line: Guide to the eye. (d) Measured (symbols) and modeled (curves) T-dependent thermal conductance G of $d = 25$ and 50 nm NWs with length $L = 12.7 \pm 0.2$ μm.

transport mechanism in the thin wires, the thermal resistance $R = 1/G$ has been plotted as a function of NW length L for diameters $d = 25$ and 50 nm in Figure 2b (main panel). For the 50 nm NWs, R is linearly dependent on L, in accordance with diffusive heat flow. For the 25 nm NWs, however, R is independent of L for all measured NWs up to $L = 15$ μm, which is proof of ballistic transport. We attribute this resistance to a small number of ballistic modes contributing to transport (see below). We note that the extrapolation of the 50 nm data goes through the origin, corroborating a negligible R_c, in agreement with a model where R_c is taken inversely proportional to the contact area between contact and NW (solid curve in Figure 2a). Although we cannot estimate R_c for the 25 nm NWs directly from the measurements, a negligible contact resistance follows from this model. The measured linear dependence of the device conduction with the number of NWs for $d = 25$ nm and $L = 6.7 \pm 0.1$ μm (inset in Figure 2b) excludes the influence of a possible background conduction. We note that these data have been collected from a device with a gap between the SiN$_x$ membranes of 4 μm, where we put down the NWs under an angle to measure NWs with $L = 6.7 \pm 0.1$ μm. We have also characterized devices with a smaller gap size of 2 μm. Also for these devices, the influence of a possible background conduction can be excluded. The data therefore unequivocally point at a

transition from diffusive to length-independent ballistic heat flow in 25 nm diameter NWs over unprecedented distances.

To further investigate the features of the diffusive-to-ballistic transition, we plot in Figure 2c (main panel) κ vs L for $d = 25$ and 50 nm NWs at 300 K, clearly showing the remarkable fact that for long wires, the thermal conductivity of the ultrathin 25 nm NWs exceeds that of the thicker 50 nm NWs. The inset displays results for 40 nm NWs at 300 and 50 K, showing that at both room and low temperature, this is a transition case: The heat flow is ballistic up to $L \approx 11$ μm and then becomes diffusive. Figure 2d shows a very weak T dependence of the thermal conductance G for both 25 and 50 nm NWs of 12.7 $\pm$ 0.2 μm length down to about 100 K (below this temperature, G steeply decreases due to phonon freeze-out). Results for 75 nm NWs are comparable to those for 50 nm NWs, showing also a very weakly T-dependent diffusive heat flow (see Figure S6). The T insensitivity rules out explanations for the diffusive-to-ballistic transition based on phonon–phonon interactions, which are strongly T dependent. In particular, Umklapp scattering, which leads to a strong decrease of κ in bulk GaP above 50 K,[25] appears to play no significant role. Also, the involvement of phonon-polaritons as heat conducting species is unlikely, because they would yield a contribution to G that is linear in T.[26] The thermal conductivities shown in Figure 2 are significantly smaller than the room-temperature thermal

conductivity of bulk GaP. For bulk GaP, experimental thermal conductivities are only available for the equilibrium zinc blende structure, with a room-temperature value of 75.2 W/m·K.[27] The calculated bulk thermal conductivity of WZ GaP is 92 ± 5 W/m·K.[28]

To substantiate the ballistic transport in the thin NWs, we probe the thermal profile of 25 and 50 nm NWs with Raman thermometry, which is a contactless method, in the same devices as used for the thermal conductivity measurements (see Figure 3a). Here, the local average lattice temperature is
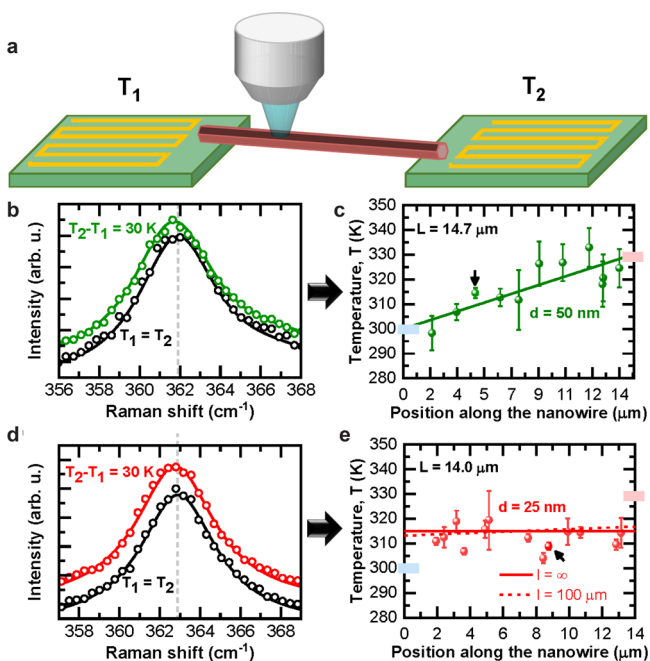

Figure 3. Temperature profiles in the diffusive and ballistic regimes. (a) Illustration of the microdevice with NW used for the measurements of the thermal profile. A laser spot is moved along the wire, and Raman spectra are acquired for $T_1 = T_2 = 300$ K and $T_1 = 300$ K, $T_2 = 300$ K + ΔT. (b) Spectra measured at the position indicated by the arrow in (c) for a NW with $d = 50$ nm and $L = 14.7 \pm 0.3$ μm. Solid lines: Lorentzian fits to the spectra. (c) Resulting temperature profile along the NW while applying $\Delta T = 30$ K using the Pt meander heaters. Solid line: Modeled profile for purely diffusive heat flow. (d) and (e) The same as (b) and (c) but for a NW with $d = 25$ nm and $L = 14.0 \pm 0.3$ μm. Solid line in (e): Modeled profile for purely ballistic transport with MFP $l = \infty$. Dashed line: Profile for $l = 100$ μm with a transmission coefficient $l/(l + L)$, having a slope $[1 - l/(l + L)]\Delta T/L$.[30] The bars at the left and right y-axis in (c) and (e) show the temperature of the contacts.

measured using the Raman shift of the transverse optical (TO) mode[29] (see Section SI6 for experimental details). We keep the system temperature at $T = 300$ K and heat the hot contact by $\Delta T = 30$ K. Swapping the contacts yields the same results (see Figure S7). The frequency shift, $\delta\omega$, of the TO mode (at about 363 cm^{-1} in GaP) with respect to the case without applying a temperature difference provides an estimate of the local lattice temperature increase, δT, since $\delta\omega \propto \delta T$ (see Figure 3b,d). This differential measurement cancels out changes in the TO mode frequency along the wire caused by other effects than the temperature difference, such as small laser heating effects and local strains. It is worth highlighting here that in the case of Stokes scattering (as we are employing), the measured spectrum reflects the average temperature of all phonon

modes, since the frequency shift of the Raman peak is the result of higher-order phonon effects and thus involves all phonon modes. In other words, our Raman experiments measure an average lattice temperature. The temperature profile along the 50 nm NW (Figure 3c) is linear, in agreement with diffusive transport. Importantly, the Raman thermometry measurements on the 50 nm NW further confirm the absence of a significant contact resistance, since the measured temperature gradient agrees with the applied temperature difference, which was calibrated in an independent manner. In the 25 nm NW (Figure 3e), however, we observe symmetric temperature jumps at the contacts and a constant temperature along the whole wire with δT close to 15 K, exactly as predicted by ballistic heat transport theory.[30] We note that the TO mode itself contributes negligibly to the heat flow because of its very short MFP, but probes the average temperature of the heat-carrying phonons. In ballistic heat flow, heat-carrying phonons traveling in either direction through the NW have the temperature of the contact from which they were injected. The lattice thermalizes equally with the "hot" and "cold" phonons, and therefore, the TO mode probes the average of the contact temperatures, that is, $\delta T = 15$ K. These results demonstrate the analogy with electrical transport through a ballistic quantum wire, where the electrical potential along the wire is constant and equal to the average of the potentials applied at the contacts.[31] To the best of our knowledge, this is the first measurement of the theoretically predicted temperature profile for ballistic heat transport. Together with the heat transport measurements of Figure 2, this provides strong experimental proof for ballistic heat flow. Interestingly, these measurements hint at the existence of a residual scattering between heat-carrying and non heat-carrying phonons.

We are not aware of an existing model in the literature that can capture a diffusive-to-ballistic transition for decreasing dimensions with the length scales involved in this work. To give a tentative explanation, we apply a model based on Landauer's formalism for phonon transport. It neglects anharmonic effects that lead to phonon–phonon scattering, in accordance with the weak T dependence of our experimental data (see insets of Figure 2c,d). The model we apply has been developed by Murphy and Moore[20] and Chen et al.[32] (see Section SI7) and was successfully used to describe heat flow in silicon NWs[32] and holey silicon.[15] It distinguishes between two different types of phonon scattering at the NW surface: The surface appears sharp (diffuse) to phonons with an inverse perpendicular wave vector component longer (shorter) than the surface oxide layer thickness, leading to mostly specular (diffuse) scattering with long (short) MFP.[20,32] This description is also consistent with Lévy walk dynamics.[18] We obtain the numbers of modes N_s and N_d of the "specular" and "diffusive" phonons at each frequency from ab initio calculations of the phonon band structure of WZ GaP and phonon subband formation in the NW (see Section SI8). In Figure S12, these numbers are plotted for $d = 25$ and 50 nm and an oxide layer thickness $h = 2.45$ nm (fitted to obtain agreement with the $d = 25$ nm thermal transport data, see below). This value of h is close to the measured thickness (see Figure 1b). We note that the number of specular phonon modes N_s is only a small fraction ($\sim 1\%$) of the number of diffusive modes N_d. We only consider phonons with a frequency below the Debye frequency. Higher-frequency phonons are hardly excited at the considered temperatures

and have too short MFPs to significantly contribute to the heat flow.

A model where both contributions of specular phonons with a strongly increased MFP and of diffusive phonons with an MFP $l = d$ are considered equally does not agree with our data (see Figure S13). The contribution of diffusive phonons in the 25 nm NWs would lead to an offset in the thermal conductivity κ, and the contribution of specular phonons in the 50 nm NWs would lead to a linear increase in κ, neither of which is observed. A suppression of the contribution to the heat flow of diffusive phonons in the 25 nm NWs accompanied by an enhancement of the contribution of specular phonons is in our model a necessary ingredient to explain the experimental data. As shown by the solid lines in Figure 2b−d, we obtain agreement with experiment both for 25 and 50 nm NWs if we: (1) neglect for the 50 nm NWs the heat flow carried by specular phonons in Landauer's expression for G (eq S4 in Section SI7) and (2) disregard for the 25 nm NWs the contribution of diffusive phonons, taking only into account the heat flow carried by specular phonons with strongly increased MFP. A finite but strongly increased MFP l up to 100 μm would still agree with the heat transport data (dashed lines in Figure 2b,c) and would result in a small temperature gradient in the 25 nm NW that is within the experimental uncertainty of the Raman measurements (dashed line in Figure 3e). Phonons in the 25 nm NWs therefore travel practically unimpeded and can truly be called ballistic. The weak T dependence of the heat transport shown in Figure 2d is explained by the fact that the main features in both N_s and N_d appear at phonon energies significantly below the thermal energy (see Figure S12). Although the original model of Murphy and Moore[20] and Chen et al.[32] makes a distinction between specular and diffusive phonons, it contains no mechanism for the suppression of the heat flow carried by diffusive phonons and the emergence of ballistic character of the specular phonons. In their model, specular phonons still undergo a weak scattering into diffusive phonon modes caused by the disordered NW surface, preventing ballisticity.

A possible cause for the suppression of the heat flow carried by diffusive phonons is Anderson localization[33] of these phonons in the 25 nm NWs. The phonon mean free paths of the diffusive phonons in the bulk WZ GaP crystal are in the range of hundreds of nanometers to several micrometers.[28] The dominant scattering of these phonons is therefore by the amorphous surface of the NW. Recent works show that in NWs with rough or amorphous surfaces, Anderson localization could take place.[34,35] The effect was shown to be increasingly important for thinner wires.[20] Another cause could be the coupling of the localized modes in the amorphous oxide layer to propagating modes in the crystalline core.[36,37] Such coupling could result in an effective layer near the boundary of the wire where the thermal conductivity is greatly reduced, an effect that can be much stronger for thinner wires. Finally, within the hydrodynamic framework,[3−5,10] the so-called no-slip condition could also lead to a strong reduction of the thermal conductivity near the boundary of the NW, quenching the contribution to the heat flow of diffusive phonons. A possible origin for the enhancement of the contribution of specular phonons and the emergence of ballisticity is a strongly reduced scattering of these phonons into diffusive modes caused by localization-induced decoupling of specular and diffusive phonons. This scenario, which would agree with the observed weak T dependence of the transition, is explained in Section SI10.

These qualitative explanations of the reduction of the contribution of diffusive phonons to the heat flow and the enhancement of the contribution of specular phonons should be quantified, such that they can be experimentally verified. Ballistic phonon transport may find application in phonon transistors,[38,39] phonon waveguides,[40] and in novel cooling solutions for computer chips, which require rapid removal of heat from ever decreasing volumes. Ballistic heat flow could possibly be realized more easily in other compound semiconductors composed of lighter elements than Ga and P, such as Al and N, because of even longer phonon MFPs.

■ ASSOCIATED CONTENT

ⓢ Supporting Information

The Supporting Information is available free of charge at https://pubs.acs.org/doi/10.1021/acs.nanolett.0c00320.

> Nanowire growth, elemental analysis, thermal conductance measurements, background conductance, diffusive heat flow in 75 nm diameter nanowires, Raman thermometry, application of Landauer's formalism for heat flow, calculation of the numbers of specular and diffusive phonon modes, contributions of specular and diffusive phonons to thermal conductivity, decoupling of specular and localized diffusive phonons (PDF)

■ AUTHOR INFORMATION

Corresponding Author

Erik P. A. M. Bakkers − *Department of Applied Physics, Eindhoven University of Technology, 5600 MB Eindhoven, The Netherlands;* ⓘ orcid.org/0000-0002-8264-6862; Email: e.p.a.m.bakkers@tue.nl

Authors

Daniel Vakulov − *Department of Applied Physics, Eindhoven University of Technology, 5600 MB Eindhoven, The Netherlands*

Subash Gireesan − *Department of Applied Physics, Eindhoven University of Technology, 5600 MB Eindhoven, The Netherlands; Center for Computational Energy Research, 5600 HH Eindhoven, The Netherlands*

Milo Y. Swinkels − *Department of Physics, University of Basel, 4056 Basel, Switzerland*

Ruben Chavez − *Department of Applied Physics, Eindhoven University of Technology, 5600 MB Eindhoven, The Netherlands*

Tom Vogelaar − *Department of Applied Physics, Eindhoven University of Technology, 5600 MB Eindhoven, The Netherlands*

Pol Torres − *Departament de Física, Universitat Autònoma de Barcelona, Bellaterra 08193, Spain*

Alessio Campo − *Department of Physics, University of Basel, 4056 Basel, Switzerland*

Marta De Luca − *Department of Physics, University of Basel, 4056 Basel, Switzerland;* ⓘ orcid.org/0000-0001-6061-3261

Marcel A. Verheijen − *Department of Applied Physics, Eindhoven University of Technology, 5600 MB Eindhoven, The Netherlands*

Sebastian Koelling − *Department of Applied Physics, Eindhoven University of Technology, 5600 MB Eindhoven, The Netherlands*

Luca Gagliano − *Department of Applied Physics, Eindhoven University of Technology, 5600 MB Eindhoven, The Netherlands;* orcid.org/0000-0003-4214-8639

Jos E. M. Haverkort − *Department of Applied Physics, Eindhoven University of Technology, 5600 MB Eindhoven, The Netherlands;* orcid.org/0000-0003-3051-673X

F. Xavier Alvarez − *Departament de Fisica, Universitat Autònoma de Barcelona, Bellaterra 08193, Spain;* orcid.org/0000-0001-6746-2144

Peter A. Bobbert − *Department of Applied Physics, Eindhoven University of Technology, 5600 MB Eindhoven, The Netherlands; Center for Computational Energy Research, 5600 HH Eindhoven, The Netherlands*

Ilaria Zardo − *Department of Physics, University of Basel, 4056 Basel, Switzerland;* orcid.org/0000-0002-8685-2305

Complete contact information is available at:
https://pubs.acs.org/10.1021/acs.nanolett.0c00320

Author Contributions

[⊥]These authors contributed equally to this work.

Notes

The authors declare no competing financial interest.

■ REFERENCES

(1) Fourier, J. B. J. *Théorie Analytique de La Chaleur*; Didot, F., Ed.; Cambridge University Press: Cambridge, 1822.

(2) Maire, J.; Anufriev, R.; Yanagisawa, R.; Ramiere, A.; Volz, S.; Nomura, M. Heat Conduction Tuning by Wave Nature of Phonons. *Sci. Adv.* **2017**, *3* (8), No. e1700027.

(3) Alvarez, F. X.; Jou, D.; Sellitto, A. Phonon Hydrodynamics and Phonon-Boundary Scattering in Nanosystems. *J. Appl. Phys.* **2009**, *105* (1), 014317.

(4) Cepellotti, A.; Fugallo, G.; Paulatto, L.; Lazzeri, M.; Mauri, F.; Marzari, N. Phonon Hydrodynamics in Two-Dimensional Materials. *Nat. Commun.* **2015**, *6*, 6400.

(5) Lee, S.; Broido, D.; Esfarjani, K.; Chen, G. Hydrodynamic Phonon Transport in Suspended Graphene. *Nat. Commun.* **2015**, *6*, 6290.

(6) Ding, Z.; Zhou, J.; Song, B.; Chiloyan, V.; Li, M.; Liu, T.-H.; Chen, G. Phonon Hydrodynamic Heat Conduction and Knudsen Minimum in Graphite. *Nano Lett.* **2018**, *18* (1), 638−649.

(7) Torres, P.; Torelló, A.; Bafaluy, J.; Camacho, J.; Cartoixà, X.; Alvarez, F. X. First Principles Kinetic-Collective Thermal Con-

ductivity of Semiconductors. *Phys. Rev. B: Condens. Matter Mater. Phys.* **2017**, *95* (16), 165407.

(8) Ziabari, A.; Torres, P.; Vermeersch, B.; Xuan, Y.; Cartoixà, X.; Torelló, A.; Bahk, J.-H.; Koh, Y. R.; Parsa, M.; Peide, D. Y.; et al. Full-Field Thermal Imaging of Quasiballistic Crosstalk Reduction in Nanoscale Devices. *Nat. Commun.* **2018**, *9* (1), 255.

(9) Martelli, V.; Jiménez, J. L.; Continentino, M.; Baggio-Saitovitch, E.; Behnia, K. Thermal Transport and Phonon Hydrodynamics in Strontium Titanate. *Phys. Rev. Lett.* **2018**, *120* (12), 125901.

(10) Beardo, A.; Calvo-Schwarzwälder, M.; Camacho, J.; Myers, T. G.; Torres, P.; Sendra, L.; Alvarez, F. X.; Bafaluy, J. Hydrodynamic Heat Transport in Compact and Holey Silicon Thin Films. *Phys. Rev. Appl.* **2019**, *11* (3), 34003.

(11) Siemens, M. E.; Li, Q.; Yang, R.; Nelson, K. A.; Anderson, E. H.; Murnane, M. M.; Kapteyn, H. C. Quasi-Ballistic Thermal Transport from Nanoscale Interfaces Observed Using Ultrafast Coherent Soft X-Ray Beams. *Nat. Mater.* **2010**, *9* (1), 26−30.

(12) Bae, M.-H.; Li, Z.; Aksamija, Z.; Martin, P. N.; Xiong, F.; Ong, Z.-Y.; Knezevic, I.; Pop, E. Ballistic to Diffusive Crossover of Heat Flow in Graphene Ribbons. *Nat. Commun.* **2013**, *4*, 1734.

(13) Hsiao, T.-K.; Chang, H.-K.; Liou, S.-C.; Chu, M.-W.; Lee, S.-C.; Chang, C.-W. Observation of Room-Temperature Ballistic Thermal Conduction Persisting over 8.3 μm in SiGe Nanowires. *Nat. Nanotechnol.* **2013**, *8* (7), 534.

(14) Wilson, R. B.; Cahill, D. G. Anisotropic Failure of Fourier Theory in Time-Domain Thermoreflectance Experiments. *Nat. Commun.* **2014**, *5*, 5075.

(15) Lee, J.; Lim, J.; Yang, P. Ballistic Phonon Transport in Holey Silicon. *Nano Lett.* **2015**, *15* (5), 3273−3279.

(16) Hu, Y.; Zeng, L.; Minnich, A. J.; Dresselhaus, M. S.; Chen, G. Spectral Mapping of Thermal Conductivity through Nanoscale Ballistic Transport. *Nat. Nanotechnol.* **2015**, *10* (8), 701.

(17) Anufriev, R.; Ramiere, A.; Maire, J.; Nomura, M. Heat Guiding and Focusing Using Ballistic Phonon Transport in Phononic Nanostructures. *Nat. Commun.* **2017**, *8*, 15505.

(18) Anufriev, R.; Gluchko, S.; Volz, S.; Nomura, M. Quasi-Ballistic Heat Conduction Due to Lévy Phonon Flights in Silicon Nanowires. *ACS Nano* **2018**, *12*, 11928.

(19) Hicks, L. D.; Dresselhaus, M. S. Thermoelectric Figure of Merit of a One-Dimensional Conductor. *Phys. Rev. B: Condens. Matter Mater. Phys.* **1993**, *47* (24), 16631.

(20) Murphy, P. G.; Moore, J. E. Coherent Phonon Scattering Effects on Thermal Transport in Thin Semiconductor Nanowires. *Phys. Rev. B: Condens. Matter Mater. Phys.* **2007**, *76* (15), 155313.

(21) Wen, Y.-C.; Hsieh, C.-L.; Lin, K.-H.; Chen, H.-P.; Chin, S.-C.; Hsiao, C.-L.; Lin, Y.-T.; Chang, C.-S.; Chang, Y.-C.; Tu, L.-W.; et al. Specular Scattering Probability of Acoustic Phonons in Atomically Flat Interfaces. *Phys. Rev. Lett.* **2009**, *103* (26), 264301.

(22) Bas, P.; Bostel, A.; Deconihout, B.; Blavette, D. A General Protocol for the Reconstruction of 3D Atom Probe Data. *Appl. Surf. Sci.* **1995**, *87*, 298−304.

(23) Shi, L.; Li, D.; Yu, C.; Jang, W.; Kim, D.; Yao, Z.; Kim, P.; Majumdar, A. Measuring Thermal and Thermoelectric Properties of One-Dimensional Nanostructures Using a Microfabricated Device. *J. Heat Transfer* **2003**, *125* (5), 881−888.

(24) Swinkels, M. Y.; van Delft, M. R.; Oliveira, D. S.; Cavalli, A.; Zardo, I.; van der Heijden, R. W.; Bakkers, E. P. A. M. Diameter Dependence of the Thermal Conductivity of InAs Nanowires. *Nanotechnology* **2015**, *26* (38), 385401.

(25) Levinshtein, M.; Rumyantsev, S.; Shur, M. *Handbook Series on Semiconductor Parameters*; World Scientific: Singapore, 1996.

(26) Ordonez-Miranda, J.; Tranchant, L.; Kim, B.; Chalopin, Y.; Antoni, T.; Volz, S. Quantized Thermal Conductance of Nanowires at Room Temperature Due to Zenneck Surface-Phonon Polaritons. *Phys. Rev. Lett.* **2014**, *112* (5), 55901.

(27) Haynes, W. M. *CRC Handbook of Chemistry and Physics*; CRC Press: Boca Raton, FL, 2014.

(28) Gireesan, S.; Torres, P.; Alvarez, F. X.; Bobbert, P. A. Diameter-Dependent Thermal Conductivity of Ultrathin GaP Nanowires: A

Molecular Dynamics Study. *Phys. Rev. B: Condens. Matter Mater. Phys.* **2020**, *101*, 024307.

(29) Olsson, K. S.; An, K.; Li, X. Magnon and Phonon Thermometry with Inelastic Light Scattering. *J. Phys. D: Appl. Phys.* **2018**, *51* (13), 133001.

(30) Maassen, J.; Lundstrom, M. Steady-State Heat Transport: Ballistic-to-Diffusive with Fourier's Law. *J. Appl. Phys.* **2015**, *117* (3), 035104.

(31) de Picciotto, R.; Stormer, H. L.; Pfeiffer, L. N.; Baldwin, K. W.; West, K. W. Four-Terminal Resistance of a Ballistic Quantum Wire. *Nature* **2001**, *411* (6833), 51.

(32) Chen, R.; Hochbaum, A. I.; Murphy, P.; Moore, J.; Yang, P.; Majumdar, A. Thermal Conductance of Thin Silicon Nanowires. *Phys. Rev. Lett.* **2008**, *101* (10), 105501.

(33) Anderson, P. W. Absence of Diffusion in Certain Random Lattices. *Phys. Rev.* **1958**, *109* (5), 1492.

(34) Xiong, S.; Sääskilahti, K.; Kosevich, Y. A.; Han, H.; Donadio, D.; Volz, S. Blocking Phonon Transport by Structural Resonances in Alloy-Based Nanophononic Metamaterials Leads to Ultralow Thermal Conductivity. *Phys. Rev. Lett.* **2016**, *117* (2), 25503.

(35) Markoš, P.; Muttalib, K. A. Phonon Localization in Nanowires Dominated by Surface Roughness. *Phys. Rev. B: Condens. Matter Mater. Phys.* **2019**, *99* (13), 134208.

(36) Xiong, S.; Selli, D.; Neogi, S.; Donadio, D. Native Surface Oxide Turns Alloyed Silicon Membranes into Nanophononic Metamaterials with Ultralow Thermal Conductivity. *Phys. Rev. B: Condens. Matter Mater. Phys.* **2017**, *95* (18), 180301.

(37) Verdier, M.; Han, Y.; Lacroix, D.; Chapuis, P.-O.; Termentzidis, K. Radial Dependence of Thermal Transport in Silicon Nanowires. *J. Phys. Mater.* **2019**, *2* (1), 015002.

(38) Wang, L.; Li, B. Thermal Logic Gates: Computation with Phonons. *Phys. Rev. Lett.* **2007**, *99* (17), 177208.

(39) Sklan, S.; Splash, R. Pop, Sizzle: Information Processing with Phononic Computing. *AIP Adv.* **2015**, *5* (5), 053302.

(40) Hatanaka, D.; Mahboob, I.; Onomitsu, K.; Yamaguchi, H. Phonon Waveguides for Electromechanical Circuits. *Nat. Nanotechnol.* **2014**, *9* (7), 520.

■ NOTE ADDED AFTER ASAP PUBLICATION

Due to a production error, this paper was published ASAP on March, 3, 2020, with an incorrect version of Figure 2. The corrected version was reposted on March 5, 2020.